Moving Beyond Monin-Obukhov Similarity Theory in Modelling Wind-Speed Profiles in the Lower Atmospheric Boundary Layer under Stable Stratification

Michael Optis, Adam Monahan, & Fred C. Bosveld

August 2014

Boundary-Layer Meteorol (2014) 153:497–514
DOI 10.1007/s10546-014-9953-z

ARTICLE

Moving Beyond Monin–Obukhov Similarity Theory in Modelling Wind-Speed Profiles in the Lower Atmospheric Boundary Layer under Stable Stratification

Michael Optis · Adam Monahan · Fred C. Bosveld

Received: 6 January 2014 / Accepted: 15 July 2014 / Published online: 2 August 2014

Abstract Monin–Obukhov similarity theory (MOST) is commonly used to model the wind-speed profile at altitudes relevant to wind-power production (e.g. 10–200 m). Though reasonably accurate for unstable to weakly stable stratification, this approach becomes less accurate under increasingly stable stratification, largely due to the constant-flux surface layer assumed by MOST becoming shallower than the altitude range of interest. Furthermore, above the surface layer, the Coriolis force has a considerable influence on the wind-speed profile (in particular in the formation of low-level jets) that cannot be modelled using similarity theory. Our goal is to compare the accuracy of alternative extrapolation models that are more physically appropriate above the surface layer. Using data from the 213-m Cabauw meteorological tower in the Netherlands between July 2007 and June 2008, it is shown that MOST is accurate only at low altitudes and low stability, and breaks down at high altitudes and high stability. Local similarity is generally more accurate than MOST across all altitudes and stabilities, though the model requires turbulent flux data at multiple altitudes that is generally impractical. In contrast, a two-layer MOST–Ekman model is found to be comparable to the other models at low stability ranges and considerably more accurate in the high stability range, while requiring only a measure of surface stability and the geostrophic wind.

Keywords Ekman layer · Monin–Obukhov similarity theory · Stable stratification · Wind power · Wind profiles

M. Optis (✉) · A. Monahan
School of Earth and Ocean Sciences, University of Victoria, P.O. Box 3065, STN CSC, Victoria, BC V8W 3V6, Canada
e-mail: optism@gmail.com

F. C. Bosveld
Royal Netherlands Meteorological Institute, De Bilt, The Netherlands

1 Introduction

1.1 Background

An accurate characterization of the near-surface wind-speed profile (up to altitudes of about 200 m) is important for a variety of wind-power applications, including wind-power resource assessment and forecasting, and estimating shear loads on turbine blades. For this purpose, the wind-power community uses a range of models of different degrees of complexity, including general circulation models (e.g. Weather Research and Forecasting model) and microscale models [e.g. Wind Atlas Analysis and Application Program (WAsP)]. However, such models can be computationally and financially expensive and may be unsuitable for situations in which quick and cost-effective methods for wind-power assessment are needed, such as the preliminary assessment of a wind-power resource from field data. For cases in which the measurement of near-surface wind speeds has been made (e.g. 10-m winds at nearby weather stations, 60-m winds at meteorological towers), the extrapolation of near-surface winds to hub-height using simple diagnostic models can often be a more practical and cost-effective approach.

The most established of these simple models follows from considering wind-speed shear within the framework of Monin–Obukhov similarity theory (MOST; Monin and Obukhov 1954), viz.

$$\phi_m\left(\frac{z}{L}\right) = \frac{\kappa z}{u_*}\frac{\partial \bar{U}}{\partial z}, \tag{1}$$

where ϕ_m is the non-dimensional wind shear, u_* is the friction velocity, $\bar{U}$ is the time-averaged wind speed, κ is the von Kármán constant (normally taken to be 0.4) and z is the height above the surface. The dimensional quantity L is the Obukhov length,

$$L = -\frac{u_*^3 \theta_s}{\kappa g \overline{(w'\theta')}_s}, \tag{2}$$

where g is the acceleration due to gravity, θ_s is the surface potential temperature, and $\overline{(w'\theta')}_s$ is the surface turbulent kinematic heat flux. Integrating Eq. 1 leads to,

$$\bar{U}(z) = \frac{u_*}{\kappa}\left[\ln\left(\frac{z}{z_0}\right) - \psi_m\left(\frac{z}{L}, \frac{z_0}{L}\right)\right], \tag{3}$$

where ψ_m accounts for the influence of stability and is derived from ϕ_m,

$$\psi_m\left(\frac{z}{L}, \frac{z_0}{L}\right) = \int_{z_0/L}^{z/L} \frac{1 - \phi_m(\zeta)}{\zeta}\,\mathrm{d}\zeta. \tag{4}$$

Although Eq. 3 is not strictly logarithmic when $\psi_m \neq 0$, we follow common practice in the literature and refer to the profile in Eq. 3 as the "logarithmic wind-speed equation". To derive Eq. 3, it is assumed that u_* and L are constant with altitude. This assumption limits the applicability of the logarithmic wind-speed profile to the atmospheric surface layer (ASL), the lowermost portion of the atmospheric boundary layer (ABL) (approximately the bottom ≈ 10 %) in which changes in the turbulent fluxes with altitude are small ($\approx$10 %) compared to their surface values. Furthermore, Eq. 3 considers only wind speed and not separate wind-vector components, and thus cannot model the rotation of the wind vector with altitude due to the Coriolis force. Within the surface layer, this rotation is generally negligible and Eq. 3 is normally found to be a good representation of the wind-speed profile (Lange and Focken 2005; Emeis 2013).

The height of the surface layer, h_{ASL}, is strongly influenced by stability. Under neutral and especially unstable conditions, vertical turbulent mixing is normally intense in the lowest few hundred metres of the ABL, resulting in h_{ASL} as great as 200 m or more (Stull 1988; Garratt 1994). Under stable stratification, the suppression of vertical turbulent mixing results in a rapid decrease of turbulent fluxes with altitude from the near-surface shear layer. Consequently, the ASL depth is significantly lower, ranging from about 20–30 m under moderately stable conditions to 1–5 m under extremely stable conditions (Stull 1988; Garratt 1994). Under these conditions, and to the extent that the assumptions of MOST are still valid (Mahrt 1998), the logarithmic wind-speed profile is valid only at very low altitudes.

Under conditions of extreme stability, turbulent fluxes become so weak and intermittent above a very shallow ASL that winds aloft decouple from the surface. Under this regime of 'z-less stratification', the turbulent flux and intensity become localized and are no longer affected by the distance from the surface, making the surface-based mixing length $l_m = \kappa z/\phi_m$ assumed by MOST an inappropriate turbulent length scale (Nieuwstadt 1984; Mahrt 1999; Mahrt and Vickers 2006; Sorbjan and Grachev 2010). In this regime, the importance of physical mechanisms other than turbulence increases. Inertial oscillations in particular have considerable influence and often lead to the formation of low-level jets (LLJs) below 200 m (Baas et al. 2009; van de Wiel et al. 2010; Banta et al. 2013). Baroclinicity can influence wind-speed shear and momentum mixing across all stabilities, while gravity waves become influential under extreme stability (Mahrt 1999; Mahrt and Vickers 2006).

Despite the limitations of the logarithmic wind-speed profile in stable conditions, it is still frequently used under these conditions for wind-power resource assessment and forecasting at altitudes within a few hundred metres of the surface. Over the last two decades, it has been used extensively in the field of wind-power meteorology (e.g. Troen and Petersen 1989; Petersen et al. 1998; Burton et al. 2001; Lange and Focken 2005; Motta et al. 2005; Berg 2008; Monteiro et al. 2009; Emeis 2010, 2013; Giebel 2011; Drechsel et al. 2012). For wind-power forecasting in particular, the logarithmic wind-speed profile has been used to interpolate wind speeds between two NWP model levels to hub-height, extrapolate observed wind speeds (e.g. tower measurements) to hub-height, or extrapolate the geostrophic winds to hub-height using the friction velocity computed from the geostrophic drag law (Tennekes 1973).

1.2 Intent and Overview of Study

The intent of this study is to assess the accuracy of several alternative simple wind-speed profile models at altitudes relevant to wind power (i.e. up to 200 m) and in conditions ranging from weakly to very stable stratification. We only consider equilibrium models in this present study, and therefore time-dependent phenomena such as LLJs cannot be modelled. The data sources used are described in Sect. 2, and the wind-speed profile models described in Sect. 3. In Sect. 4, methods used to determine model parameters are described, and results of the model comparison are shown in Sect. 5. A discussion is provided in Sect. 6, and conclusions in Sect. 7.

2 Data Sources

This study makes use of data obtained from the Cabauw Meteorological Tower in the Netherlands, operated by the Royal Netherlands Meteorological Institute (KNMI). Measurements of meteorological variables at 10-min resolution were obtained from July 1 2007 to June 30

2008 (these data are available at http://www.cesar-database.nl). Wind speed and direction measurements are made at 10, 20, 40, 80, 140, and 200 m, and temperature measurements are made at these altitudes as well as 2 m. Surface pressure measurements are also provided, which are used to calculate the potential temperature at different heights. Turbulent momentum and kinematic heat-flux measurements made at altitudes of 5, 60, 100 and 180 m are provided by KNMI. Surface geostrophic wind components at 1-h resolution derived from surface pressure measurements in the regional vicinity of Cabauw are provided by KNMI and are linearly interpolated to 10-min resolution. Observations for which 200-m wind speeds <5 m s^{-1} are excluded from the analysis (representing 22 % of the data). Under these conditions, the flux–gradient relationships are known to perform poorly (Mahrt 1998). Furthermore, low wind-speed conditions are not of interest for wind-power applications, so the accuracy of different wind-speed profile models under these conditions is not relevant in the present context.

3 Description of Alternative Wind-Speed Profile Models

Here, we introduce different wind-speed profile models considered in this analysis, as well as the data needed to use them for wind-speed extrapolation.

3.1 Local Similarity

Local similarity (Nieuwstadt 1984; Sorbjan 1988; Sorbjan and Grachev 2010) is an extension of MOST above the surface layer. Its basic premise is that non-dimensionalized turbulence statistics at a given altitude can be determined based on local observations in the same way that statistics for the ASL are based on surface observations in MOST. This concept is applied only in stable conditions, as turbulent transport in unstable conditions can be highly non-local. Sorbjan (1988) argued that the forms of the similarity functions for local similarity and MOST should be identical, so the wind-speed profile between two nearby altitudes can be expressed as

$$\bar{U}(z_2) = \bar{U}(z_1) + \frac{\sqrt{(\tau/\rho_0)_l}}{\kappa}\left[\ln\left(\frac{z_2}{z_1}\right) - \psi_m\left(\frac{z_2}{L_l}, \frac{z_1}{L_l}\right)\right], \tag{5}$$

where $(\tau/\rho_0)_l$ and L_l correspond to the local momentum flux and Obukhov length, respectively, and $z_2 > z_1$. As with MOST, local similarity is based on the assumption of continuous turbulence and becomes invalid for weak and intermittent turbulence (i.e. very stable conditions). Therefore, local similarity should be least accurate in the upper stability regimes (though not as inaccurate as MOST). In this context, local similarity provides an upper limit to the accuracy of similarity-based logarithmic wind-speed profile modelling, and serves as a useful benchmark for comparing other wind-speed profile models.

3.2 Gryning Model

Modifications to the logarithmic wind-speed profile applicable within the entire ABL were proposed by Gryning et al. (2007) and applied in a number of subsequent studies (e.g. Gryning and Batchvarova 2008; Pena et al. 2010; Sathe et al. 2011, 2012; Kumar and Sharan 2012). Gryning et al. (2007) proposed two key modifications: the first replaces u_* in Eq. 1 with an altitude-dependent turbulent momentum flux, expressed as a linear function of u_* and the ABL height, h_{ABL} (Panofsky 1973),

$$\sqrt{\tau(z)/\rho_0} = u_* \left(1 - \frac{z}{h_{ABL}}\right). \tag{6}$$

The second modification replaces the surface-layer form $l_m = \kappa z/\phi_m$ in Eq. 1 with a generalized form of the Blackadar (1962) mixing length,

$$l_m(z) = \kappa \left(\frac{\phi_m(\frac{z}{L})}{z} + \frac{1}{L_{MBL}} + \frac{1}{h_{ABL} - z}\right)^{-1}. \tag{7}$$

The first term in Eq. 7 results in the standard MOST mixing length for small values of z; the second term is a mid-boundary-layer mixing length (with $L_{MBL} << h_{ABL}$) that places an upper bound on the magnitude of l_m. This term is set as a constant or is parametrized by other means (e.g. through the geostrophic drag law in Gryning et al. 2007). The final term results in the mixing length decreasing to zero at the top of the ABL, above which turbulence should normally be negligible. Integrating the non-dimensional wind-speed shear equation with these new parametrizations and using the Dyer and Hicks (1970) form $\phi_m = 1 + \beta z/L$ (with $\beta = 5$), Gryning et al. (2007) derive the following modified equation for stable conditions,

$$\bar{U}(z) = \frac{u_*}{\kappa}\left[\ln\left(\frac{z}{z_0}\right) + \beta\frac{z}{L}\left(1 - \frac{z}{2h_{ABL}}\right) + \frac{z}{L_{MBL}} - \frac{z^2}{2h_{ABL}L_{MBL}}\right]. \tag{8}$$

Results from Gryning et al. (2007) and subsequent studies (e.g. Pena et al. 2010; Emeis 2013) have demonstrated the ability of the modified model to provide more accurate wind-speed profiles within the ABL under all stabilities compared to the standard MOST approach.

The assumptions of the Gryning model limit its application under conditions of stable stratification. First, the model is by construction applicable at heights below h_{ABL}. Under stable conditions, h_{ABL} is relatively small and may not be well-defined (e.g. Stull 1988; Seidel et al. 2010). For very stable conditions, Gryning et al. (2007) find an average $h_{ABL} \approx 60$ m, and above $z = 60$ m the model cannot be applied. Second, although the proposed asymptotic formulation of l_m is appropriate for neutral and unstable conditions, it is unable to capture the very low mixing lengths observed in very stable stratification. The L_{MBL} value typically ranges between 40 and 150 m. In stable conditions l_m can be significantly smaller above the ASL, as low as even 1 m in extremely stable conditions (Stull 1988). A more appropriate scaling of L_{MBL} may be a linear dependence on the surface Obukhov length (Delage 1974; Stull 1988) which would result in lower l_m values and would still result in an analytical expression for $\bar{U}(z)$ as in Eq. 8. Other limits for l_m under stable stratification include the Osmodov length or buoyancy length scale (Stull 1988), although neither of these result in an analytic expression for $\bar{U}(z)$. Finally, the Gryning model is still founded on similarity principles, and thus cannot model the rotation of the wind vector due to the increased influence of the Coriolis force in stable conditions.

3.3 Ekman Layer and Two-Layer Models

Turbulent fluxes within the stable ABL are generally parametrized as diffusion processes (e.g. $\overline{u'w'} = -K_m \partial\bar{u}/\partial z$, with K_m the diffusivity coefficient). In general, K_m increases approximately linearly with height in the ASL, reaches a maximum above the surface layer and decreases asymptotically to zero at the top of the ABL. A common idealized approach is to approximate K_m as constant above the ASL (the so-called Ekman layer), which results in a 'two-layer' model in which K_m increases linearly in the ASL up to h_{ASL} and remains constant above. Within the Ekman layer, considering the balance between the pressure-gradient force,

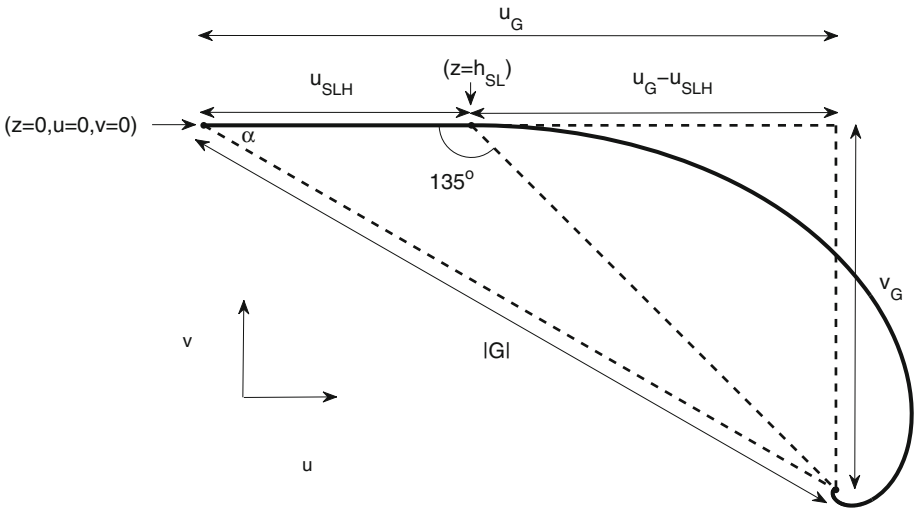

Fig. 1 Wind hodograph of the two-layer model used in this analysis (adapted from Blackadar 1998). The co-ordinate system is aligned with the ASL winds such that $v_{ASL} = 0$. The wind vector increases from (0, 0) at the surface to $(u_{SLH}, 0)$ at h_{ASL} with constant wind direction under a MOST-based logarithmic profile. Above h_{ASL}, the wind vector rotates along the Ekman spiral asymptoting to the geostrophic values u_G and v_G. The angle between the near-surface wind and the geostrophic wind vectors is denoted α. When $\alpha = 0°$, the wind profile is described entirely by the MOST-based logarithmic profile. When $\alpha = 45°$, the wind profile is described entirely by the Ekman layer model

the Coriolis force and the turbulent momentum-flux divergence, and assuming stationarity, results in the well-known Ekman layer equations,

$$u(z) = u_G + (u_{BC} - u_G)\mathrm{e}^{-\gamma z_T}\cos(\gamma z_T) + (v_{BC} - v_G)\mathrm{e}^{-\gamma z_T}\sin(\gamma z_T), \tag{9a}$$

$$v(z) = v_G + (v_{BC} - v_G)\mathrm{e}^{-\gamma z_T}\cos(\gamma z_T) - (u_{BC} - u_G)\mathrm{e}^{-\gamma z_T}\sin(\gamma z_T), \tag{9b}$$

where u_G and v_G are the geostrophic wind vector components, u_{BC} and v_{BC} are the components of the wind vector at some specified lower boundary z_{BC} (for example, taken to be the surface where the flow vanishes), $\gamma = \sqrt{f/(2K_m)}$, and $z_T = z - z_{BC}$. The Ekman layer model can be used to describe the entire wind-vector profile (i.e. $z_{BC} = 0$) or can be used within a two-layer MOST–Ekman framework (i.e. $z_{BC} = h_{ASL}$). A hodograph representation of this two-layer model is shown in Fig. 1 (Blackadar 1998). By accounting for the Coriolis force, the Ekman layer equations result in the rotation of the wind vector with altitude (the so-called Ekman spiral). The geometry of the Ekman spiral is such that a tangent at any point along the spiral in Fig. 1 makes a 45° angle with the vector joining this point to the geostrophic wind vector (Blackadar 1998), as shown in Fig. 1. Consequently, the angle α between the wind below $z = h_{ASL}$ and the geostrophic wind is between 0 and 45°. The Ekman layer profile is then a special case of the two-layer model when $h_{ASL} = 0$ and $\alpha = 45°$. Provided K_m is sufficiently small (in conditions of weak turbulence, such as under stable stratification), both the Ekman layer and two-layer models result in low altitude maxima in the wind-speed profile (evaluated to occur at $z = 2.28\gamma^{-1} + z_{BC}$). Furthermore, the Ekman layer equations are particularly appealing in cases of surface decoupling (i.e. very stable conditions), since the winds are not determined entirely by the near-surface wind.

The Ekman layer model has been used as an idealization in introductory studies of the ABL (Stull 1988; Garratt 1994; Blackadar 1998; Etling 2002; Emeis et al. 2007; Donda et al. 2013)

as well as recent conceptual studies of stable ABL phenomena such as LLJs (van de Wiel et al. 2010; Baas et al. 2012). The two-layer model was discussed in Blackadar (1998) in the context of deriving the geostrophic-drag law. Emeis et al. (2007) and Emeis (2013) applied this two-layer model for wind-speed profile modelling up to hub-height in non-neutral conditions,

$$U(z) = \begin{cases} (u_*/\kappa)\left[\ln(z/z_0) - \psi_m(z/L, z_0/L)\right], & z < h_{ASL} \\ G\left[\cos(\alpha) - \sin(\alpha)\right], & z = h_{ASL} \\ G[1 - 2\sqrt{(}2)\mathrm{e}^{-\gamma(z-h_{ASL})}\sin(\alpha)\cos(\gamma(z - h_{ASL}) & \\ +\pi/4 - \alpha) + 2\mathrm{e}^{-2\gamma(z-h_{ASL})}\sin^2(\alpha)]^{1/2} & z > h_{ASL} \end{cases} \tag{10}$$

where G is the magnitude of the geostrophic wind vector. The expression for $U(z)$ for the case $z = h_{ASL}$ follows from Fig. 1, while the expression for $U(z)$ for the case $z > h_{ASL}$ follows from the Ekman layer equations (Eq. 9).

By equating the MOST-based and Ekman-based wind speeds and their vertical gradients at the interface h_{ASL}, Emeis (2013) derived two expressions relating the internal parameters of the model,

$$u_* = \frac{\kappa G\left(\cos(\alpha) - \sin(\alpha)\right)}{\ln(h_{ASL}/z_0) - \psi_m(h_{ASL}/L, z_0/L)}, \tag{11}$$

$$u_* = \frac{2G\gamma\kappa h_{ASL}\sin(\alpha)}{\phi_m(h_{ASL}/L)}. \tag{12}$$

In Emeis (2013), $h_{ASL} = 150$ m and $L = -200$ m were specified for daytime and $h_{ASL} = 30$ m and $L = 150$ m for nighttime conditions. Equations 11 and 12 were then solved for α and u_*, and the resulting mean wind-speed profiles were compared to those from MOST-based and Gryning et al. (2007) models over an urban area using 1 month of data. The results of this earlier study showed that the two-layer model provided the most accurate mean wind-speed profiles of all the models considered. While Emeis (2013) demonstrated the potential of this model, important issues were not addressed: the values of h_{ASL} and L were not justified, the sample size was relatively small (i.e. 1 month of data), and no indication of scatter in individual wind-speed profiles (e.g. standard deviation, root-mean-squared error) was provided. The present study extends the earlier results of Emeis (2013).

4 Methods

Having described the different wind-profile models, we now describe the application of these models to the problem of wind-speed extrapolation. We consider model performance within different stability regimes based on the bulk Richardson number determined between 200 m and the surface (Table 1),

$$Ri_B = \frac{g}{\theta_{avg}}\frac{z_{200}(\theta_{200} - \theta_{surf})}{U_{200}^2}, \tag{13}$$

where θ_{avg} is the mean potential temperature across all measurement altitudes between 2 and 200 m. Temperature measurements at 2 m are used for the surface values. The Beljaars and Holtslag (1991) functional forms for ψ_m and ψ_h (the similarity function for heat) in stable conditions are used throughout the analysis, as these forms were derived using Cabauw data,

$$\psi_m = -a\left(\frac{z}{L} - \frac{z_0}{L}\right) - b\left(\frac{z}{L} - \frac{c}{d}\right)\exp\left(-d\frac{z}{L}\right) + b\left(\frac{z_0}{L} - \frac{c}{d}\right)\exp\left(-d\frac{z_0}{L}\right), \tag{14}$$

Table 1 Stability regime ranges used throughout this analysis, based on Ri_B between 200 m and the surface

Stability regime	Ri_B criteria	Occurrence (%)
Unstable	$Ri_B < 0$	15.1
Weakly stable	$0 < Ri_B < 0.05$	29.2
Moderately stable	$0.05 < Ri_B < 0.15$	23.3
Very stable	$0.15 < Ri_B < 0.5$	22.0
Extremely stable	$Ri_B > 0.5$	10.4

Table 2 Summary of models considered in this analysis, including observed and prescribed input parameters as well as internally computed parameters

Model	Observed input parameters	Internally computed parameters
MOST (local z_0)	U_{10}, z_0, $Ri_{B,surf}$	L_{surf}, ψ_m
Local similarity	U_{10}, τ_5, τ_{60}, τ_{100}, τ_{180} L_5, L_{60}, L_{100}, L_{180}	ψ_m
Gryning	U_{10}, z_0, $Ri_{B,surf}$, G	u_*, L_{surf}, h_{ABL}, ϕ_m, ψ_m
Ekman layer	U_{10}, τ_{100}, G	u_G, v_G, γ
Two-layer	U_{10}, $Ri_{B,surf}$, G	z_0, u_*, L_{surf}, h_{ASL}, α, u_G v_G, ϕ_m, ψ_m, γ
MOST (effective z_0)	U_{10}, $Ri_{B,surf}$, G	z_0, L_{surf}, ψ_m

Numbered subscripts denote the height of the observed parameter

$$\psi_h = -\left(1+\frac{2}{3}a\frac{z}{L}\right)^{3/2} + \left(1+\frac{2}{3}a\frac{z_0}{L}\right)^{3/2} - b\left(\frac{z}{L}-\frac{c}{d}\right)\exp\left(-d\frac{z}{L}\right) + b\left(\frac{z_0}{L}-\frac{c}{d}\right)\exp\left(-d\frac{z_0}{L}\right) \tag{15}$$

with $a = 1$, $b = 2/3$, $c = 5$, and $d = 0.35$. One exception is the Gryning model (Eq. 8), which by construction uses the simplified Dyer and Hicks (1970) form of ϕ_m that keeps the number of terms of Eq. 8 to a minimum.

Both the input observational data as well as the methods used to determine internal parameters vary between models. A summary of observed and prescribed input parameters as well as internally computed parameters for each model is shown in Table 2. We now turn to more detailed descriptions of the methods used.

4.1 Correcting for Internal Boundary Layers

The immediate surroundings at Cabauw (within 200 m) are relatively flat while farther away from the tower (within 1–2 km) surface roughness increases significantly due to the presence of small towns and belts of trees (Verkaik and Holtslag 2007). This effect produces internal boundary layers (IBLs) in the flow around Cabauw, and in particular results in lower than expected turbulent flux values near the surface compared to higher altitudes (a detailed discussion of IBL effects at Cabauw is provided in Verkaik and Holtslag 2007). This effect is demonstrated in Fig. 2, in which mean turbulent flux profiles of momentum and heat at Cabauw are displayed along with the corresponding median Obukhov length profile. The median is displayed to reduce the influence of very small values of $|L|$ when $u_* << 1$ m s^{-1}.

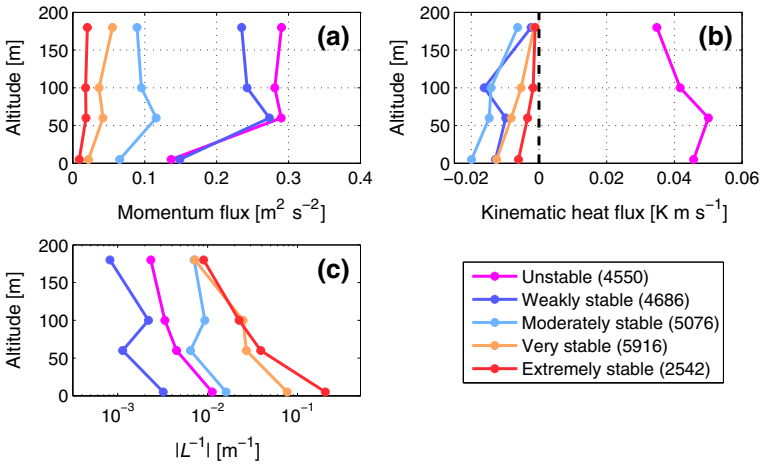

Fig. 2 Vertical profiles of: **a** mean turbulent momentum flux, **b** mean turbulent kinematic heat flux, and **c** median $|L^{-1}|$ for the stability regimes described in Table 1

As seen in Fig. 2a, the momentum fluxes do not decrease monotonically with altitude, as would be expected on average for horizontally homogeneous conditions. Rather, the fluxes at 5 m are lower than those at 60 m across all stability regimes. The effect of IBLs at Cabauw is evident in the kinematic heat-flux profile for unstable and weakly stable conditions (Fig. 2b) but not for the other stability regimes, which show a monotonic decrease in magnitude with altitude. The lower momentum flux near the surface results in lower magnitudes of the surface Obukhov length (Fig. 2c). Consequently, the use of a surface flux-derived Obukhov length in the logarithmic wind-speed profile (Eq. 3) overestimates the magnitude of stability aloft. To correct for the influence of IBLs in extrapolating wind speeds using Eq. 3, we iteratively solve for the 'bulk' Obukhov length at the surface, L_{surf}, using the surface bulk Richardson number, $Ri_{B,surf}$, measured between 10 m and z_0,

$$Ri_{B,surf} = \left(\frac{10}{L_{surf}}\right) \frac{\ln\left(\frac{10}{z_0}\right) - \psi_h\left(\frac{10}{L_{surf}}, \frac{z_0}{L_{surf}}\right)}{\left[\ln\left(\frac{10}{z_0}\right) - \psi_m\left(\frac{10}{L_{surf}}, \frac{z_0}{L_{surf}}\right)\right]^2}, \tag{16}$$

where 2-m air temperatures are used as surface values. Using this approach, the Obukhov length is effectively 'tuned' to be compatible with the particular z_0 used. Numerous methods exist for determining z_0 by wind direction, with a large range of values depending on the method (Verkaik and Holtslag 2007). Different choices of z_0 result in substantially different extrapolated wind-speed profiles, and we found that using z_0 values provided by KNMI that describe local roughness in 2.5° segments based on land-use maps, provided accurate wind-speed profiles up to 80 m for the weakly stable case (i.e. conditions in which the assumptions of MOST are expected to be valid). These z_0 values are thus used in this analysis.

A comparison of the surface-flux measured L to the bulk-derived L_{surf} is shown in Fig. 3 for stable conditions. As shown therein, the bulk-derived approach generally results in larger values of L_{surf} (i.e. more neutral) compared to the surface flux-derived values, thus providing some correction for the influence of IBLs. One possible reason for this correction is that temperatures at 2 and 10 m adjust less rapidly to the underlying surface than does the turbulence at 5 m, and therefore are more representative of upstream roughness. The

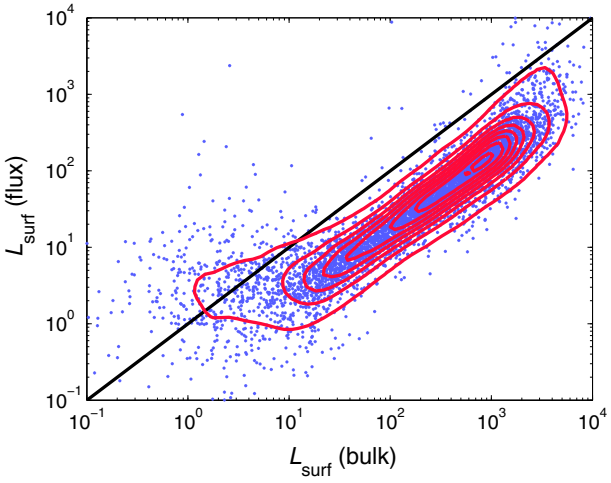

Fig. 3 Scatter plot of surface-flux-derived Obukhov length at 5 m and surface bulk Richardson-number-derived Obukhov length. Also contoured are kernel density estimates of the joint probability density function of the logarithm of these two variables. Contour lines denote boundaries within which 5 % (inner)–95 % (outer) of the data are contained, and are contoured in 10 % increments

populations of the two variables in Fig. 3 largely follow a line parallel to the 1:1 line and can therefore be connected by a multiplicative factor. An exception to this relationship occurs for low values of L_{surf} (i.e. very stable), for which low near-surface wind speeds result in low values of $\Delta U/\Delta z$ and therefore high values of $Ri_{B,surf}$.

4.2 MOST (Local z_0)

The bulk-derived L_{surf} and the z_0 values based on local land-use maps are used to extrapolate 10-m wind speeds using MOST. Specifically, we extrapolate 10-m wind speeds to a height z by taking the ratio of Eq. 3 at z and Eq. 3 at 10 m,

$$\bar{U}(z) = \bar{U}_{10} \frac{\left[\ln\left(\frac{z}{z_0}\right) - \psi_m\left(\frac{z}{L_{surf}}, \frac{z_0}{L_{surf}}\right)\right]}{\left[\ln\left(\frac{10}{z_0}\right) - \psi_m\left(\frac{10}{L_{surf}}, \frac{z_0}{L_{surf}}\right)\right]} \tag{17}$$

4.3 Local Similarity

For the local similarity model, momentum fluxes and flux-derived Obukhov lengths measured at 5, 60, 100, and 180 m are linearly interpolated to the mid-points between wind measurement altitudes (i.e. 15, 30, 60, 100, and 170 m). Wind speeds at 20 m are calculated from 10-m wind speeds and 15-m fluxes, after which 40-m wind speeds are calculated from 20-m wind speeds and 30-m fluxes, and so on. For all cases, we use the Beljaars and Holtslag (1991) similarity function (Eq. 14) for locally stable conditions and, for locally unstable conditions,

$$\psi_m(\zeta) = \frac{\pi}{2} - 2\arctan(x) + \log\frac{(1+x)^2(1+x^2)}{8} \tag{18}$$

with $x = (1-16\zeta)^{1/4}$.

4.4 Gryning Model

The z_0 and L_{surf} values used in the MOST (local z_0) model are also used for the Gryning model. The remaining parameters h_{ABL} and L_{MBL} are parametrized using the same approach in Pena et al. (2010); specifically, h_{ABL} takes the form (Tennekes 1973),

$$h_{ABL} = C\frac{u_*}{f}, \tag{19}$$

where C is a constant. Different values of C are used based on L_{surf}, as in Pena et al. (2010). The L_{MBL} value is determined by equating the Gryning wind-speed profile (Eq. 8) at $z = h_{ABL}$ to the geostrophic wind as expressed by the geostrophic drag law,

$$G = \frac{u_*}{\kappa}\sqrt{\left[\ln\left(\frac{u_*}{f z_0}\right) - A\right]^2 + B^2}. \tag{20}$$

Different values of A and B are used based on L_{surf}, as in Pena et al. (2010).

4.5 Ekman Layer Model

For the Ekman layer model, a bottom boundary condition of 10 m (i.e. $z_T = 10$ m, $u_{BC} = u_{10}$, $v_{BC} = v_{10}$ in Eq. 9) is used to be consistent with the other extrapolation approaches. Appropriate use of the Ekman layer model requires that the geostrophic wind is rotated 45° to the surface wind vector (Fig. 1). Since the observed 10-m and geostrophic winds are not in fact generally separated by this angle, we define an 'effective' geostrophic wind vector with the same magnitude of the observed surface geostrophic wind vector but rotated appropriately. We parametrize the diffusivity coefficient K_m based on momentum-flux measurements at 100 m (i.e. $K_m = D\tau/(\rho_o f)$, with D a constant), assuming that flux data at 100 m best represent atmospheric conditions in the bottom 200 m of the ABL. It was found that a value of $D = 4 \times 10^{-3}$ provided the most accurate wind profiles in the higher stability regimes (in which the Ekman layer model is expected to be most valid) and is used in this analysis. The Ekman layer model breaks down when $G < U_{10}$, which occurs in 2.3 % of the data. These data are excluded from analysis.

4.6 Two-Layer Model

For the two-layer model, U_{10}, $Ri_{B,surf}$ and G are input parameters, while the remaining five parameters (z_0, u_*, L_{surf}, h_{ASL}, and α) are solved iteratively using the following system of equations: Eqs. 3 and 16 at 10 m, Eqs. 11–12, and a final equation describing h_{ASL} as a function of the other parameters. Zilitinkevich (1975) applied Rossby similarity theory in stable conditions to derive an expression for h_{ABL} as a function of the dimensionless parameter $\mu = u_*/(fL)$,

$$h_{ABL} = \frac{au_*}{f}F(\mu), \tag{21}$$

where a is a constant, au_*/f is the height of the ABL in neutral conditions, and $F(\mu)$ is a function that must be specified. We assume that h_{ASL} scales likewise in stable conditions and use the same functional form as in Zilitinkevich (1975). Numerical experiments carried out with a single-column momentum budget model assuming horizontal homogeneity and no advection suggest the following expression for h_{ASL},

$$h_{ASL} = \frac{bu_*}{f}F(\mu) \tag{22}$$

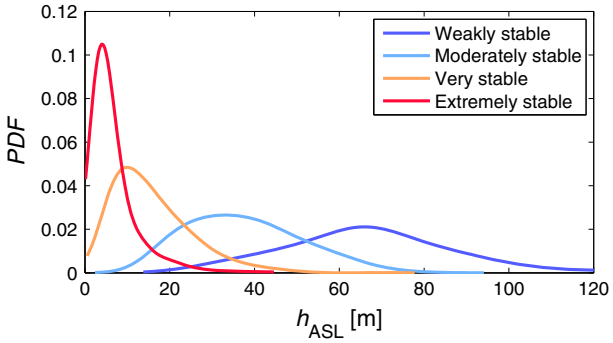

Fig. 4 PDFs of h_{ASL} for different stability regimes, as determined from Eq. 22

with $b = 0.0127$ and $F = \left(1 + 0.011\mu + 0.022\mu^2\right)^{-1/4}$. Probability density functions (PDFs) of h_{ASL} as determined from the two-layer model are shown in Fig. 4 for the different stability regimes. In the weakly stable case, there is a broad range of h_{ASL} values extending up to roughly 120 m; low values correspond to weak winds and high values correspond to strong winds. The range is much narrower in the extremely stable case, with values extending up to roughly 40 m. The peak in the PDF at about 5 m corresponds to frequent periods of strongly stable stratification, for example during summer nights.

Having determined the complete set of two-layer model parameters, we first extrapolate the 10-m wind speeds up to h_{ASL} using the logarithmic wind-speed equation (Eq. 17). The wind speed at h_{ASL} then becomes the boundary condition for the Ekman layer equations (Eq. 9) that are applied above h_{ASL}. The constant diffusivity coefficient K_m for the Ekman layer is determined using the MOST formulation evaluated at h_{ASL},

$$K_m(h_{ASL}) = \frac{u_* \kappa h_{ASL}}{\phi_m \left(\frac{h_{ASL}}{L_{surf}}\right)}. \tag{23}$$

As was done for the Ekman layer model, we determine an 'effective' geostrophic wind vector that has the same magnitude of the observed surface geostrophic wind and is rotated by the angle α (as determined from the two-layer system of equations) to the 10-m wind vector. Similar to the Ekman layer model, cases in which $G < U_{10}$ are excluded from analysis. For cases in which $h_{ASL} < 10$ m (18.8 % of the cases), the two-layer system effectively reduces to an Ekman layer model for a 10–200 m extrapolation. For these cases, the MOST-derived form of K_m (Eq. 23) is not appropriate for modelling the flow aloft, and in particular results in excessively low values of K_m due to the large magnitude of the ϕ_m term. For these cases, a formulation for K_m is used based on u_* as determined from the two-layer system of equations. It was found that $K_m = 0.0017 u_*^2 / f$ provided the most accurate results in extremely stable conditions and is used here.

4.7 MOST (Effective z_0)

The final model is equivalent to the MOST (local z_0) model but uses the z_0 and L_{surf} values determined from the two-layer system. We include this model to provide a direct comparison of the MOST and two-layer models using the same parameters.

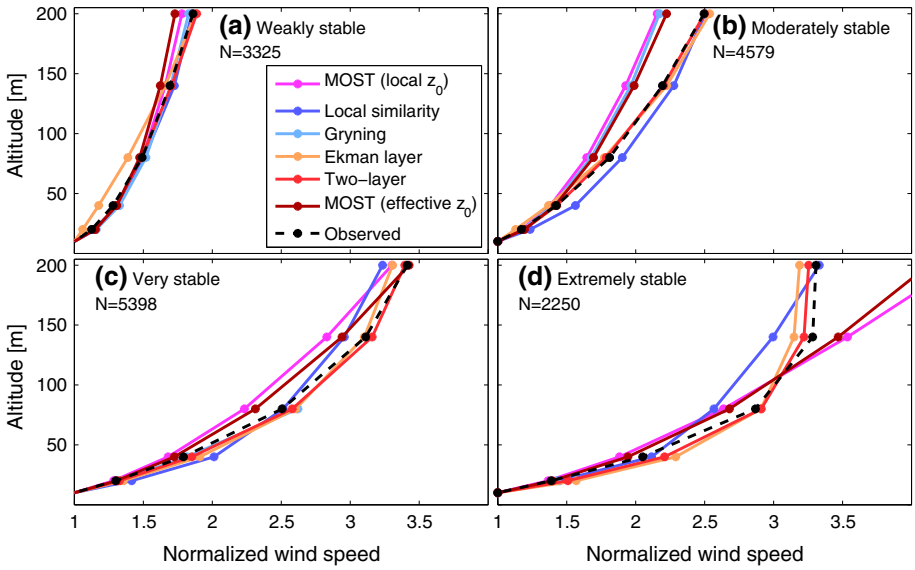

Fig. 5 Modelled and observed mean wind-speed profiles for the different stability regimes

5 Results

We now assess the performance of the different wind-profile models described in the previous section under different stability conditions. Each wind-speed profile model uses different sets of data that are subject to data gaps that occur at different times and altitudes. To make meaningful comparisons between models, only time intervals for which the required observational data are available for all the models are considered. Since the Gryning model is invalid when $z > h_{ABL}$, we limit the Gryning wind profile up to 80 m in very stable conditions and up to 20 m in extremely stable conditions, while the remaining wind-profile models are extrapolated up to 200 m across all stability regimes.

In Fig. 5, observed and modelled mean wind-speed profiles (normalized to 10-m winds) under different stability regimes are compared. In general, lower wind-speed shear is observed in the lower stability ranges and higher wind-speed shear is observed in the higher stability ranges. In the extremely stable range, the mean wind speeds at 140 and 200 m are close in value, reflecting frequent cases of LLJs. Most models under consideration are accurate up to 200 m in the weakly stable case, except for the Ekman layer model, which due to high values of K_m tends to underestimate wind speeds. The MOST models tend to underestimate wind speeds at the higher altitudes. There is considerably higher divergence in the modelled profiles in the moderately stable regime (Fig. 5b). Both MOST models and the Gryning model underestimate wind speeds, while the local similarity model tends to slightly overestimate wind speeds. Both the Ekman layer and two-layer models are accurate at all altitudes. Similar results are found for the very stable regime (Fig. 5c), apart from the local similarity model that tends to underestimate wind speeds at higher altitudes. The breakdown of MOST is evident in the extremely stable case (Fig. 5d), in which both MOST models substantially overestimate wind speeds at higher altitudes. Local similarity is accurate up to 50 m but underestimates wind speeds at higher altitudes. The two-layer and Ekman layer models slightly overestimate wind speeds at lower altitudes and slightly underestimate wind speeds at higher altitudes,

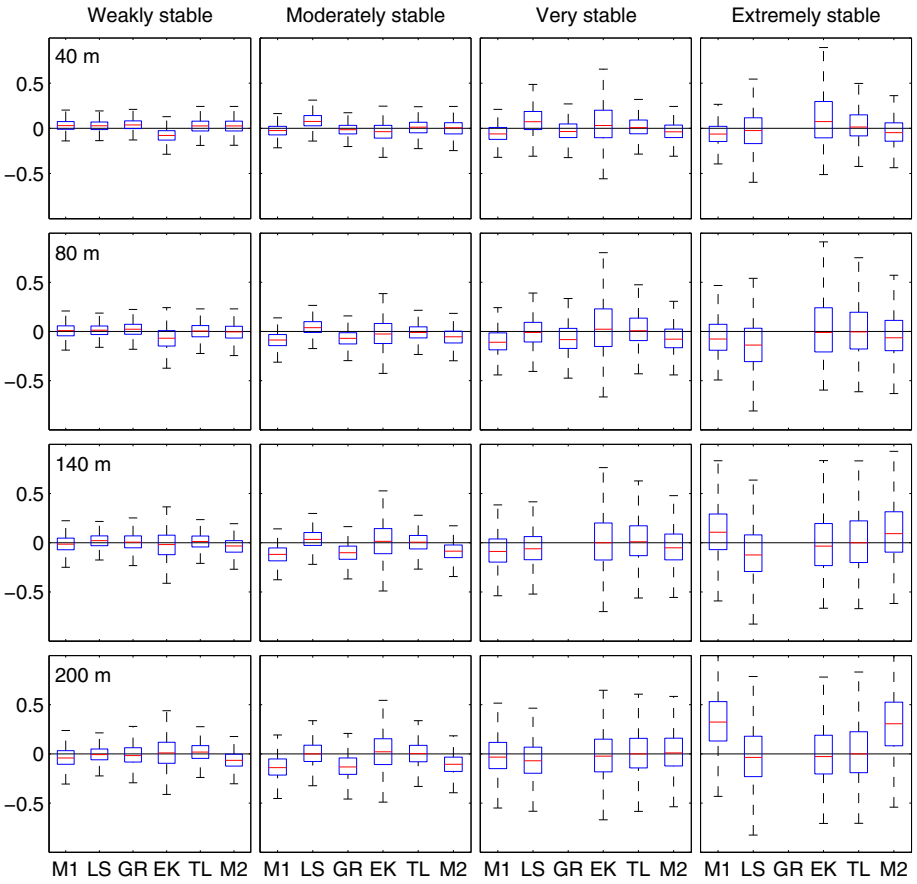

Fig. 6 Box plots of the percentage error between modelled and observed winds (i.e. $(U_{mod} - U_{obs}) / U_{obs}$) at different altitudes (*rows*) and stability regimes (*columns*). The *red lines* show the mean values, *blue boxes* show the interquartile range, and *black dotted lines* show the total range excluding outliers. Acronyms for the different models are as follows: *M1* MOST (local z_0), *LS* local similarity, *GR* Gryning, *EK* Ekman layer, *TL* two layer, *M2* MOST (effective z_0)

though both models still accurately account for the general shape of the observed wind-speed profile.

Box plots of the percentage error between modelled and observed winds (i.e. $(U_{mod} - U_{obs}) / U_{obs}$) at different altitudes and stability regimes are shown in Fig. 6. In general, the spread of the model predictions around the observed wind speeds increases with stability and altitude. At lower altitudes and low stability (i.e. upper-left quadrant in Fig. 6), the spread is relatively comparable between models, apart from the Ekman layer model that shows the highest spread. A similar trend is observed at lower altitudes and high stability (i.e. upper-right quadrant in Fig. 6), with the MOST (local z_0) model generally showing the least spread. At higher altitudes and low stability (i.e. lower-left quadrant in Fig. 6), the Ekman layer model shows the greatest spread while the other models have comparable spread. At higher altitudes and extreme stability, the MOST models show the greatest spread while the remaining models show comparable spread.

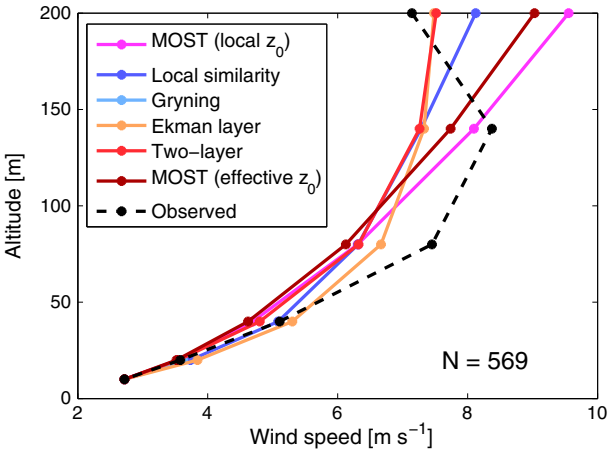

Fig. 7 Modelled and observed mean wind-speed profiles for cases in which an LLJ is observed

Modelled and observed mean wind-speed profiles for cases in which an LLJ is observed are shown in Fig. 7. We identify an LLJ event when either the 10-min averaged 80-m or 140-m wind speeds are at least 10 % greater than the 200-m wind speed. As shown in Fig. 7, none of the models is able to accurately model the wind profile in the presence of pronounced LLJs. Similarity-based models are by construction unable to do so, as these cannot simulate a decrease in wind speed with altitude. The Ekman layer and two-layer models (which can model a decrease in wind speed with altitude) tend to underestimate wind shear and on average do not produce a LLJ. Furthermore, both the Ekman layer and two-layer models are equilibrium models (i.e. no time dependence) whereas the LLJ is a time-dependent phenomenon, so the inability of these models to accurately account for the LLJ is expected.

6 Discussion

This analysis has demonstrated that the two-layer model results in wind-speed profiles that are of similar accuracy to other models in conditions of weakly stable stratification but become substantially better as the stability increases. Local similarity was accurate in all but the extremely stable regime and was the most data intensive of all the models, requiring flux data at multiple altitudes. Such data are rarely available in the field, and thus the practical use of the local similarity model is limited. Though the Gryning model showed some improvement over the MOST (local z_0) model, its limited altitude range of applicability limits its practical use in very to extremely stable conditions. The two-layer model required only a measure of the geostrophic wind (readily available through surface pressure observations) and a measure of surface stability. Among all the models, the two-layer model provided the best balance of low bias, low variance, and minimal input data for the entire stability range.

The different approaches to determining z_0 used in this analysis emphasize the role of z_0 more as a tunable boundary-condition parameter than a value with an unambiguous physical meaning. For the MOST (local z_0) model, we used z_0 values based on local land-use data to obtain accurate results for the wind profile at low altitudes. As a consequence, the model was inaccurate in the upper stability ranges and at higher altitudes. Had we instead used

regional z_0 values, accuracy at higher altitudes would have improved, but accuracy at lower altitudes would have decreased. For the two-layer model, z_0 values were solved within the system of equations with knowledge only of the 10-m wind speed, geostrophic wind speed and surface stability. No explicit relation between z_0 and wind direction was required, in contrast to conventional land-use-based z_0 approaches (Verkaik and Holtslag 2007).

Despite its improved accuracy relative to other models, the two-layer model remains a highly idealized representation of lower ABL physics. The forms $K_m = D\tau_{100}/(\rho_0 f)$ used for the Ekman layer model and $K_m = 0.0017u_*^2/f$ used for the upper stability limit of the two-layer model are rather simplified and contribute to the large scatter in model results, particularly in the higher stability regimes in which $u_*^2 << 1$ m^2 s^{-2}. More comprehensive forms of K_m (e.g. a function of $F(\mu)$ as in Rossby similarity theory) would likely lead to improved accuracy in the wind profiles. The limit in accuracy of the two-layer model under these improved parametrizations can be explored by comparing its results to a single-column momentum budget model that uses more comprehensive representations of ABL turbulence (though advection is still neglected). More detailed and physically appropriate parametrizations for K_m should result in more accurate wind-speed profiles. Such a comparison will be the subject of future studies.

Another limitation of the two-layer and Ekman layer models is the frequent inconsistencies between surface-pressure-derived geostrophic wind data and tower data. For example, for unstable conditions with $U_{200} > 10$ m s^{-1} (for which h_{ASL} should be near or above 200 m), in 26.5 % of the observations the surface geostrophic wind speed was less than the wind speed at 200 m. In this study, we assumed that the geostrophic winds were constant with altitude, neglecting the possibility of baroclinic conditions in which geostrophic wind speeds at 200 m may have differed from those at the surface by several m s^{-1}. The use of surface temperature measurements along with pressure measurements to obtain estimates of both the surface pressure-gradient force and the temperature gradient would allow for a baroclinic correction to these models. Alternatively, the use of pressure level winds from global or regional models at appropriate altitudes would also provide a better representation of the geostrophic flow above the surface.

All models considered in this analysis are based on equilibrium or steady-state conditions. This is a reasonable approximation in the unstable, neutral and weakly stable ABL in which the ABL adjustment time scales are short (on the order of 1h or less) (Mahrt 2014). However, the steady-state assumption breaks down for the moderate to extremely stable ABL. The formation and evolution of the LLJ at sunset is one striking example. Over the course of the night, inertial oscillations cause wind vectors aloft to oscillate around their equilibrium value with an amplitude equal to the degree of departure from equilibrium around the moment of surface decoupling (van de Wiel et al. 2010). In some cases, the magnitude of the oscillation can be several m s^{-1}. As shown in this study, the equilibrium two-layer model was not accurate in the presence of LLJs. Time dependence can be incorporated into the two-layer approach by retaining the time dependence in the idealized force-balance equation (e.g. van de Wiel et al. 2010). Future studies will assess the ability of the two-layer approach to accurately model the evolution of the LLJ under such conditions.

7 Conclusions

We have considered the accuracy of various wind-profile models up to heights of 200 m in stable conditions using meteorological data from the 213-m tower at Cabauw. The logarithmic wind-speed profile (based on Monin–Obukhov similarity theory) was found to be reasonably

accurate up to moderately stable conditions but became increasingly inaccurate for more stable stratification due to the surface layer becoming shallower. Local similarity-based profiles showed considerable improvement across all stability ranges, but were substantially more data intensive. A fundamental limitation of any model based on similarity theory is that it cannot account for the influence of the Coriolis force under strong stability and weak turbulence. The Ekman layer model based on fluxes measured at 100 m was shown to be more accurate than similarity approaches in the higher stability range. The two-layer MOST–Ekman model provided the best balance of low bias and variance for the entire stability range, and required only the geostrophic wind and surface bulk Richardson number as input parameters. These results present a compelling case for the use of a two-layer model in wind-power resource assessment and forecasting.

References

Baas P, Bosveld FC, Baltink HK, Holtslag A (2009) A climatology of nocturnal low-level jets at Cabauw. J Appl Meteorol Climatol 48(8):1627–1642

Baas P, van de Wiel B, van den Brink L, Holtslag A (2012) Composite hodographs and inertial oscillations in the nocturnal boundary layer. Q J R Meteorol Soc 138(663):528–535

Banta RM, Pichugina YL, Kelley ND, Hardesty RM, Brewer WA (2013) Wind energy meteorology: insight into wind properties in the turbine-rotor layer of the atmosphere from high-resolution Doppler Lidar. Bull Am Meteorol Soc 94(6):883–902

Beljaars A, Holtslag A (1991) Flux paramterization over land surfaces for atmospheric models. J Appl Meteorol Climatol 30(3):327–341

Blackadar A (1962) The vertical distribution of wind and turbulent exchange in a neutral atmosphere. J Geophys Res 67(8):3095–3102

Blackadar A (1998) Turbulence and diffusion in the atmosphere. Springer, New York, 185 pp

Burton T, Sharpe D, Jenkins N, Bossanyi E (2001) Wind energy handbook. Wiley, New York, 780 pp

Delage Y (1974) A numerical study of the nocturnal atmospheric boundary layer. Q J R Meteorol Soc 100(425):351–364

Donda JMM, Van de Wiel BJH, Bosveld FC, Beyrich F, van Heijst GJF, Clercx HJH (2013) Predicting nocturnal wind and temperature profiles based on external forcing parameters. Boundary-Layer Meteorol 146(1):103–117

Drechsel S, Mayr GJ, Messner JW, Stauffer R (2012) Wind speeds at heights crucial for wind energy: measurements and verification of forecasts. J Appl Meteorol Climatol 51(9):1602–1617

Dyer A, Hicks B (1970) Flux–gradient relationships in constant flux layers. Q J R Meteorol Soc 96(410):715–721

Emeis S (2010) A simple analytical wind park model considering atmospheric stability. Wind Energy 13(5):459–469

Emeis S (2013) Wind energy meteorology—atmospheric physics for wind power generation. Springer, Dordrecht, 150 pp

Emeis S, Baumann-Stanzer K, Piringer M, Kallistratova M, Kouznetsov R, Yushkov Y (2007) Wind and turbulence in the urban boundary layer—analysis from acoustic remote sensing data and fit to analytical relations. Meteorol Z 16(4):393–406

Etling D (2002) Theoretische Meteorologie Eine Einfuhrung, 2nd edn. Springer, Berlin, 376 pp

Garratt JR (1994) The atmospheric boundary layer. Cambridge University Press, UK, 316 pp

Giebel G (2011) The state-of-the-art in short term prediction of wind power—a literature overview, 2nd edn. ANEMOS, 109 pp

Gryning S-E, Batchvarova E (2008) Modelling of the urban wind profile. In: Borrego C, Miranda A (eds) Air pollution modeling and Its application XIX, NATO Science for Peace and Security Series Series C: Environmental Security. Springer, Dordrecht, pp 18–27

Gryning S-E, Batchvarova E, Bruemmer B, Jorgensen H, Larsen S (2007) On the extension of the wind profile over homogeneous terrain beyond the surface boundary layer. Boundary-Layer Meteorol 124(2):251–268

Kumar P, Sharan M (2012) Parameterization of the eddy diffusivity in a dispersion model over homogeneous terrain in the atmospheric boundary layer. Atmos Res 106(0):30–43

Lange M, Focken U (2005) Physical approach to short-term wind power prediction. Springer, Berlin, 167 pp

Mahrt L (1998) Stratified atmospheric boundary layers and breakdown of models. Theor Comput Fluid Dyn 11(3–4):263–279
Mahrt L (1999) Stratified atmospheric boundary layers. Boundary-Layer Meteorol 90(3):375–396
Mahrt L (2014) Stably stratified atmospheric boundary layers. Annu Rev Fluid Mech 46:23–45
Mahrt L, Vickers D (2006) Extremely weak mixing in stable conditions. Boundary-Layer Meteorol 119(1):19–39
Monin AS, Obukhov AM (1954) Basic laws of turbulence mixing in the surface layer of the atmosphere. Q J R Meteorol Soc 24:163–187
Monteiro C, Bessa R, Miranda V, Botterud A, Wang J, Conzelmann G (2009) Wind power forecasting: state-of-the-art 2009. Argonne National Laboratory, 216 pp
Motta M, Barthelmie R, Volund P (2005) The influence of non-logarithmic wind speed profiles on potential power output at Danish offshore sites. Wind Energy 8(2):219–236
Nieuwstadt F (1984) The turbulent structure of the stable, noctural boundary layer. J Atmos Sci 41(14):2202–2216
Panofsky H (1973) Tower micrometeorology. In: Haugen DA (ed) Workshop on micrometeorology. American Meteorological Society, Boston, pp 151–176
Pena A, Gryning S, Hasager C (2010) Comparing mixing-length models of the diabatic wind profile over homogeneous terrain. Theor Appl Climatol 100(3–4):325–335
Petersen EL, Mortensen NG, Landberg L, Hjstrup J, Frank HP (1998) Wind power meteorology. Part I: climate and turbulence. Wind Energy 1(1):2–22
Sathe A, Gryning S-E, Pea A (2011) Comparison of the atmospheric stability and wind profiles at two wind farm sites over a long marine fetch in the North Sea. Wind Energy 14(6):767–780
Sathe A, Mann J, Barlas T, Bierbooms WAAM, van Bussel GJW (2012) Influence of atmospheric stability on wind turbine loads. Wind Energy 16:1013–1032
Seidel DJ, Ao CO, Li K (2010) Estimating climatological planetary boundary layer heights from radiosonde observations: comparison of methods and uncertainty analysis. J Geophys Res 115(D16)
Sorbjan Z (1988) Structure of the stably-stratified boundary layer during the SESAME-1979 experiment. Boundary-Layer Meteorol 44(3):255–266
Sorbjan Z, Grachev A (2010) An evaluation of the flux–gradient relationship in the stable boundary layer. Boundary-Layer Meteorol 135(3):385–405
Stull R (1988) An introduction to boundary-layer meteorology. Kluwer, Dordrecht, 670 pp
Tennekes H (1973) Similarity laws and scale relations in planetary boundary layers. In: Workshop on micrometeorology. American Meteorological Soceity, pp 177–216
Troen I, Petersen E (1989) European wind atlas. Riso National Laboratory, Roskilde, 656 pp
Van de Wiel B, Moene A, Steeneveld G, Baas P, Bosveld F, Holtslag A (2010) A conceptual view on inertial oscillations and nocturnal low-level jets. J Atmos Sci 67(8):2679–2689
van den Berg G (2008) Wind turbine power and sound in relation to atmospheric stability. Wind Energy 11(2):151–169
Verkaik J, Holtslag A (2007) Wind profiles, momentum fluxes and roughness lengths at Cabauw revisited. Boundary-Layer Meteorol 122(3):701–719
Zilitinkevich SS (1975) Resistance laws and prediction equations for the depth of the planetary boundary layer. J Atmos Sci 32:741752